catalysts

MDPI

Article

An Aging Model of NH_3 Storage Sites for Predicting Kinetics of NH_3 Adsorption, Desorption and Oxidation over Hydrothermally Aged Cu-Chabazite

Selmi Erim Bozbag [1], Deniz Şanlı [2], Barkın Özener [2], Gökhan Hisar [2] and Can Erkey [1,*]

[1] Department of Chemical and Biological Engineering, Koç University, Sarıyer, 34450 Istanbul, Turkey; sbozbag@ku.edu.tr

[2] Ford Otosan R&D Center, Sancaktepe, 34885 Istanbul, Turkey; dsanliyi@ford.com.tr (D.S.); bozener@ford.com.tr (B.O.); ghisar@ford.com.tr (G.H.)

* Correspondence: cerkey@ku.edu.tr; Tel.: +90-212-339-1866

Received: 31 January 2020; Accepted: 16 February 2020; Published: 8 April 2020

Abstract: A unified transient kinetic model which can predict the adsorption, desorption and oxidation kinetics of NH_3 over hydrothermally aged Cu-chabazite was developed. The model takes into account the variation of fractional coverages of NH_3 storage sites due to hydrothermal aging. In order to determine the fractional coverage of these sites, the catalyst was aged for various times at a certain temperature followed by NH_3 adsorption, desorption and temperature-programmed desorption (TPD) experiments. TPD profiles were deconvoluted mainly into three peaks with centres at 317, 456 and 526 °C, respectively. Hydrothermal aging resulted in the progressive increase in the intensity of the peak at 317 °C and decrease in the intensity of the peaks at 456 and 526 °C, along with decreased NH_3 oxidation at high temperatures. A model for hydrothermal aging kinetics of the fractional coverage of storage sites was developed using three reactions with appropriate rate expressions with parameters regressed from experimental data. The model was then incorporated into a multi-site kinetic model for the degreened Cu-Chabazite by the addition of aging reactions on each storage site. The effects of both aging time and temperature on the kinetics NH_3 adsorption, desorption and oxidation were successfully predicted in the 155-540 °C range. This study is the first step towards the development of a hydrothermal aging-unified kinetic model of NH_3-Selective Catalytic Reduction over Cu-chabazite.

Keywords: kinetic model; hydrothermal aging; NH_3-TPD; Cu-Chabazite; Cu-SSZ-13; adsorption; desorption; oxidation; NH_3-SCR

1. Introduction

An engine aftertreatment system (ATS) of a heavy-duty vehicle comprises an NH_3-Selective Catalytic Reduction (NH_3-SCR) reactor in which NOx and NH_3 react to form N_2 and H_2O via a variety of reactions including Standard, Fast and NO_2-SCR. Cu-Chabazite (CHA) is the catalyst of choice due to its good deNOx performance and better high temperature stability as compared to other Cu-zeolites [1]. Much-speculated upcoming Euro7 emission regulations will impose more stringent NOx emission standards than before and also restrict CO_2 emissions. The latter would indeed require increasing the combustion efficiency of the engine by lowering engine outlet temperatures, which would lower SCR efficiencies. Therefore, intense engineering efforts are directed towards the design, calibration and control of the SCR reactors in the future ATSs of heavy-duty vehicles with lean burn diesel engines. The design and calibration of SCR reactors is usually carried out using data from engine dynamometer and vehicle tests that scan a large operation region of the engine. However, such tests are very long,

labour intensive and expensive. Alternatively, mathematical models for SCR reactors which consist of mass, heat and momentum transport equations for the gas and solid phases in the reactors could be used [2–4].

An important consideration in the development of such models is the decrease in catalytic activity with time on stream due to exposure to high temperatures in the presence of water vapour, particularly during the regeneration of diesel particulate filters. For example, for SCR reactors which utilize Cu-CHA, NOx conversion decreases in a low temperature range (<250 °C), initially increases and then decreases in the high temperature range (>450 °C) with increasing HA temperature. Moreover, NH_3 oxidation and NO oxidation performances also decrease [5–9]. The effects of this phenomena, called hydrothermal aging (HA), need to be incorporated to SCR reactor models to be able to predict the long-term performance and calibrate the ATS in such a way to ensure the meeting of emission regulations during the lifetime of the vehicle.

In order to develop a reactor model capable of predicting the deNOx performance of both de-greened and aged SCR catalysts, a good understanding of the nature of active sites and their reactions throughout the lifetime of the catalyst is required. However, this is an extremely difficult task due to two factors. Firstly, the active sites of the degreened Cu-CHA and the reaction mechanism are already quite complex. Along this line, efforts are concentrated on elucidating the NH_3-SCR chemistry on Cu-zeolites using kinetic experiments, spectroscopy and theoretical calculations [10–17]. These efforts revealed one of the most intriguing and complicated catalytic mechanisms ever reported for Cu-SSZ -13 [18], where active Cu sites with dynamic mobility under NH_3 solvation react with NOx under a redox cycle. Studies with Cu-CHAs showed different reaction mechanisms and kinetics in at least two regimes below 250 °C and above 330 °C [12], in which different Cu species were active with different reactivity where Brönsted sites (ZH) acted as an additional NH_3 reservoir, which improved deNOx performance [19]. A number of redox-capable species, i.e, mono-atomic copper-oxo ($ZCu^{II}OH$, on the eight-membered ring (MR) of the SSZ-13) [16,20–23], dicopper species [24] and copper species with dynamic mobility in NH_3 solvation [18,23,25] for the low temperature regime (<250 °C) were proposed. Surprisingly, the apparent standard SCR rate reached a peak in the temperature range 300-330 °C which was followed by a decreased rate as the temperature was further inceased [26]. This was ascribed to the loss of mobility of the Cu sites which link more to the zeolitic framework as the temperature was raised above 300 °C [27] and the presence of other Cu species (such as Z_2Cu^{II}), most probably on the 6 MR with reduced redox capability [23,26]. The mechanism by which the latter species is consumed during the high temperature SCR is much less understood. The oxidation of NH_3 over Cu-CHA is another important factor affecting deNOx performance, particularly above 300 °C, and is included in SCR kinetic models. Again based on spectroscopic and kinetic modelling studies, Z_2Cu^{II} and $ZCu^{II}OH$ site are believed to be responsible for NH_3 oxidation at temperatures below and above 300 °C, respectively [28,29], with significantly different rates [12,30]. These findings are usually taken into account while developing kinetic models for NH_3-SCR process over degreened Cu-CHA. These models usually consist of a multi-reaction scheme which includes NH_3 adsorption/desorption, NH_3 oxidation, NO oxidation, Standard-SCR, Fast-SCR, NO_2-SCR, N_2O and NH_4NO_3 formation reactions and their rate expressions to account for the effects of temperature, NO_2/NOx ratio and NH_3/NOx ratio (ANR) on product distribution. In most of these kinetics models, which are either single or multisite, the active site concentration was obtained by NH_3 adsorption/temperature-programmed desorption (TPD) experiments by assuming a one to one stoichiometry between NH_3 and active sites or was obtained by fitting the model to experimental data [31–45]. Alternatively, active Cu site concentration could also be obtained directly using H_2-TPR [46], transient response techniques [47] or XAS [26]. The other difficulty in the development of such a model is to account for the changes in the reaction mechanism due to changes in active site speciation upon HA.

Kinetic models which account for hydrothermal aging are scarce in the literature [48]. These only work at specific aging conditions and extrapolation between models is necessary to accurately predict the performance of hydrothermally aged catalysts. Recently, Ruggeri et al. found a linear correlation

between the ammonia storage capacity loss and the corresponding changes in the pseudo-first-order rate constants of the two reactions most affected by aging, i.e., ammonia oxidation and standard SCR, during the hydrothermal aging process for Fe-zeolite [49]. The developed aging model was able to describe effectively all their experimental data, collected at different aging times and aging temperatures, on a predictive basis. The study concluded that such an approach may also be applicable to other types of catalyst formulations. A similar treatment cannot be easily carried out for Cu-CHA since the total NH_3 storage does not change up to very long aging times. There have also been studies on the effects of aging on the nature and concentration of active sites on Cu-CHA which do not involve kinetic models. It has been found that the resistance of Cu-CHA to HA is due to the exceptional hydrothermal stability of the Z_2Cu^{II} sites located on 6MR, which also act as structure stabilizers during HA [50–52] and prevent dealumination. HA mostly affects the $ZCu^{II}OH$ sites which in turn convert to CuO_x clusters [9,50,53] and cause some dealumination [28,54], and clusters in turn grow and destroy the zeolite cage [55] resulting in activity loss with hard HA. For mild aging, these changes in catalyst performance were attributed to the changes in the concentration of the individual active Cu sites. In a pioneering study on aging, Luo et al. proposed that $ZCu^{II}OH$ reacted with ZH to produce Z_2Cu^{II} and water upon HA, based on the behaviour of NH_3-TPD profiles. A consistent increase in the intensity of the lower temperature peak around 300 °C and a decrease in the intensity of the higher temperature peaks (>400 °C) were observed. The decrease in the intensity of higher temperature peaks was attributed to the decrease in the Brönsted sites, whereas the increase of the 300 °C peak was attributed to the formation of new Z_2Cu^{II} sites which were assumed to accommodate more NH_3 per Cu than $ZCu^{II}OH$ [56,57]. The changes in the active site concentrations upon HA were also supported by H_2-TPR and DRIFTS studies [56]. Recently, the same group were able to link the HA kinetics of the active sites to a transient kinetic model of NH_3 adsorption and desorption of fresh Cu-CHA in order to simulate the NH_3-TPD profiles of the aged catalysts. This was based on the mean-field approximation, implying constant turnover Arrhenius rate constants for the adsorption and desorption reactions, but with changing individual site densities directly affecting the rates associated with the aforementioned reactions [58]. However, it has also been shown that via H_2-TPR, NH_3-TPD, DRIFTS [29,30,50] and in situ time-resolved XAS [26] that the NH_3-TPD profiles of Cu-CHA are much more complicated than proposed in [56]. Additionally, the multi-site kinetic models to predict deNOx performance [30,44,59] suggest that the highest temperature peak of NH_3-TPD profile of Cu-CHA is associated with NH_3 desorption from $ZCu^{II}OH$ sites residing at the 8MR.

Despite the numerous spectroscopic and kinetic studies on the issue, it appears that there is no unambiguous agreement as to which species are responsible for which TPD peak and there is a need for more detailed analysis and kinetic modelling of the NH_3-TPD profiles of degreened Cu-CHA. Moreover, there is no report in the literature on the kinetic modelling of HA effects coupled with NH_3 storage and oxidation models of the degreened catalysts to predict the performance over hydrothermally aged Cu-CHA. Here, a HA-unified transient kinetic model which can predict the NH_3 adsorption breakthrough, isothermal desorption of NH_3 and NH_3-TPD behaviors upon HA between 650–800 °C range up to 46h, is presented for Cu-CHA. Using this model, the NH_3 oxidation performance in the 155–540 °C range, from its freshly degreened state up to the mild HA state (in the 650–800 °C range, up to 46h of isothermal HA), is predicted for the first time in the literature, based on the kinetic parameters of the degreened catalyst. For this purpose, an HA kinetics model consisting of four NH_3 storage sites, was developed by determining the changes in fractional coverage of these sites by deconvoluting experimental NH_3-TPD data only. Then, the active site HA kinetics model was coupled with the transient kinetic model for the degreened Cu-CHA while keeping the turnover rate constants and activation energies associated with adsorption, desorption and oxidation reactions unchanged upon HA.

2. Results and Discussion

2.1. Hydrothermal Aging Kinetics of NH_3 Storage Sites

Figure 1 shows a typical profile for the adsorption, isothermal desorption and TPD of NH_3 over degreened Cu-CHA. The TPD profile was fitted with four Gaussian peaks associated with different NH_3 storage sites, hereafter referred to as ZCu1, ZCu2 and ZB, with peak centers at 317, 456 and 526 °C, respectively, along with a small contribution from Z_2W with a peak center at 126 °C. Z_2W site is associated with sites on which either physically adsorbed NH_3 [30] or $Cu(NH_3)_4$ species with very low or no reactivity towards SCR related reactions reside [26]. Its concentration was obtained by adding the amount of NH_3 desorbed during the isothermal desorption period and the amount desorbed corresponding to the small peak with the center at 126 °C. ZCu1 and ZCu2 are associated with Cu sites responsible for SCR-related reactions commonly referred to as Z_2Cu^{II} and $ZCu^{II}OH$, which reside at the 6 and 8 MRs, respectively [23]. ZB sites are associated with Brönsted sites that were not exchanged with Cu during catalyst synthesis.

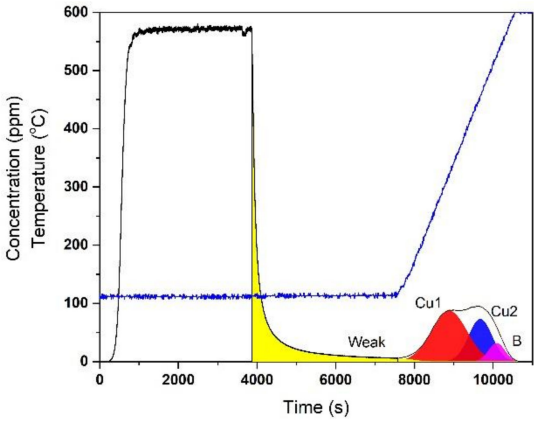

Figure 1. Deconvolution of NH_3 desorption data of the degreened Cu-CHA.

Figure 2 shows the NH_3-TPD profiles for Cu-CHA with increasing aging times at 650, 700 and 800 °C. The intensity of the peaks in the higher temperature region of the curves decreased and the intensity of the peaks in the lower temperature region increased with increasing time, in line with the observations in the literature [57]. Meanwhile, the total NH_3 storage stayed nearly constant with increasing aging time at all the temperatures investigated in this study (Figure 2d).

Figure 3 illustrates the peaks obtained from the deconvolution of the data in Figure 2. The peaks are associated with Z_2W, ZCu1, ZCu2 and ZB sites. Data clearly show the rapid decrease in the intensity of the peak associated with ZB, a much slower decrease in the intensity of the peak associated with ZCu2 and an increase in the intensity of the peak associated with ZCu1 with increasing times of HA.

Figure 4 shows the changes in the fractional coverages of sites with time (Figure 4a,c,e) along with the sequential HA and NH_3 adsorption/TPD sets. HA sets given in Figure 4b,d,f are for durations of 109, 60 and 50 h (i.e., totals of 46, 25 and 21 h isothermal HA at 650, 700 and 800 °C, respectively, heating and cooling ramps, and also includes the time required for NH_3 adsorption and TPD experiments). After HA at 650 °C (Figure 4a), the fractional coverage of ZCu1 slightly decreased and then increased with time to reach a value 28% higher than the degreened one, whereas the coverage of ZCu2 slightly increased by 12%, and then decreased with time to reach a value 22% lower than the degreened one. Initial changes in fractional coverages upon HA indicates that the initial degreening treatment (550 °C, 2 h) was not enough to produce the maximum possible concentration of ZCu2. Cu mobility during HA is a very complex process where both Cu sites can interchange among themselves up to a saturation in Cu2 concentration. The rate of initial increase in fractional coverage of ZCu2 with aging time was higher than its rate of decrease due to HA. Meanwhile, the fractional coverage of ZB decreased much faster than the fractional coverage of ZCu2, indicating that the decay mechanism for these two species

could be different during HA. The fractional coverage of Z_2W initially increased slightly and then stayed constant throughout. For runs at 700 °C (Figure 4c) and 800 °C (Figure 4e), the initial decrease and increase in the fractional coverages of ZCu1 and ZCu2 were not observed, most probably because this process is happening much faster than HA kinetics. Similar to the data at 650 °C, fractional coverage of ZCu1 increased with time whereas fractional coverage of ZCu2 and ZB decreased. Again, the decay rates of ZB were much faster than those of ZCu2.

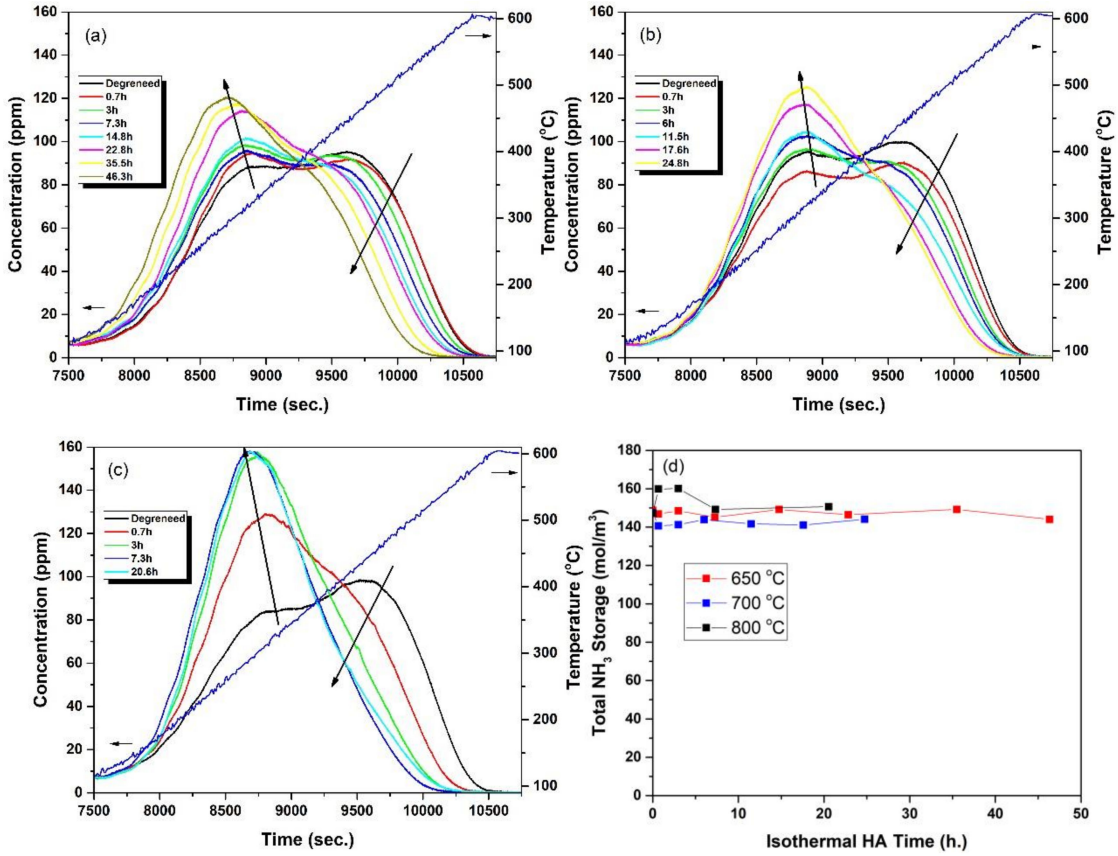

Figure 2. Variation of temperature-programmed desorption (TPD) profiles for Cu-CHA with aging times at (**a**) 650 °C, (**b**) 700 °C, (**c**) 800 °C, (**d**) Variation in the total site concentration with aging time at different temperatures. Insets in (**a**–**c**) show the cumulative isothermal hydrothermal aging (HA) times.

Based on the above observations, three reactions for describing the changes in fractional coverages with aging time were proposed. The reactions for aging and their rate expressions are shown in Table 1 (Reactions 1–3). The main reaction responsible for HA is Reaction 3, where ZCu2 sites convert to ZCu1. The reaction responsible for the decrease in coverage of ZB, and initial decrease and increase of coverages of ZCu1 and ZCu2, respectively, was Reaction 2. Since two empty sites (Z) were used as reactants in Reaction 2, an empty Z site was formed. It was assumed that this site was converted to Z_2W via reacting with ZCu1, as given by Reaction 1, to describe the slight increase in coverage of Z_2W upon HA. Equation (12) (given in Section 3.3.1) was written for each surface species (Z_2W, ZCu1, ZCu2, ZB) using the rate expressions for Reactions 1–3. Rate equation parameters were then regressed from fractional coverage versus time data given in Figure 4 and are presented in Table 2. Model results are in excellent agreement with the measured values at all times and at each aging temperature. Thus, all of the changes in fractional coverages of Z_2W, ZCu1, ZCu2 and ZB with aging time were predicted very well at each aging temperature. The HA reaction mechanism in [56] was also investigated in this study using elementary rate laws. However, the mechanism in [56] was not able to describe accurately the HA data obtained in this study. Particularly, that model could not describe the fast decrease in

fractional coverage of ZB with aging time and rather slow decrease in fractional coverage of ZCu2 at longer times.

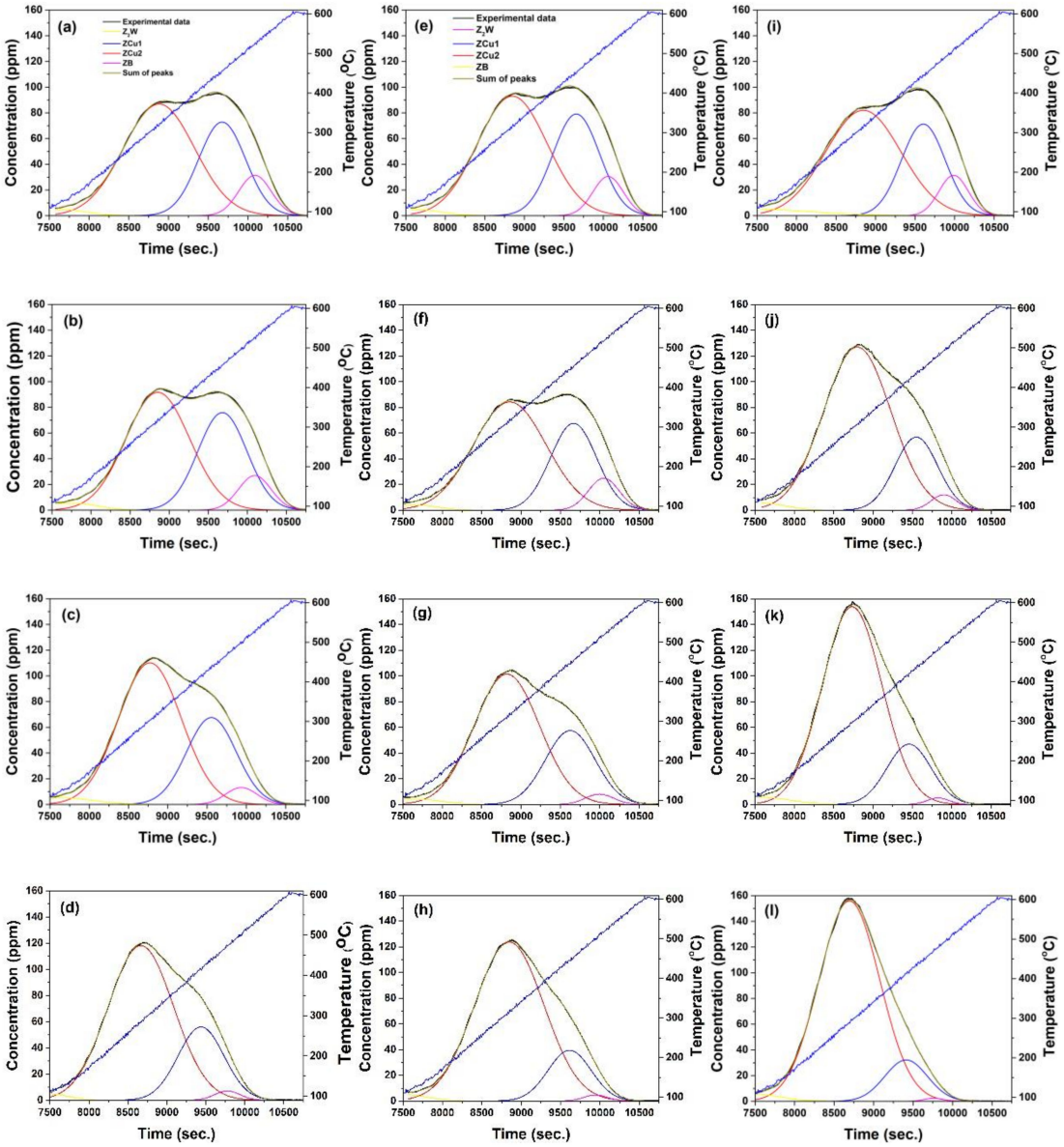

Figure 3. Deconvolution of TPD profiles after successive HA steps (**a**–**d**) 650 °C, (**e**–**h**) 700 °C, (**i**–**l**) 800 °C.

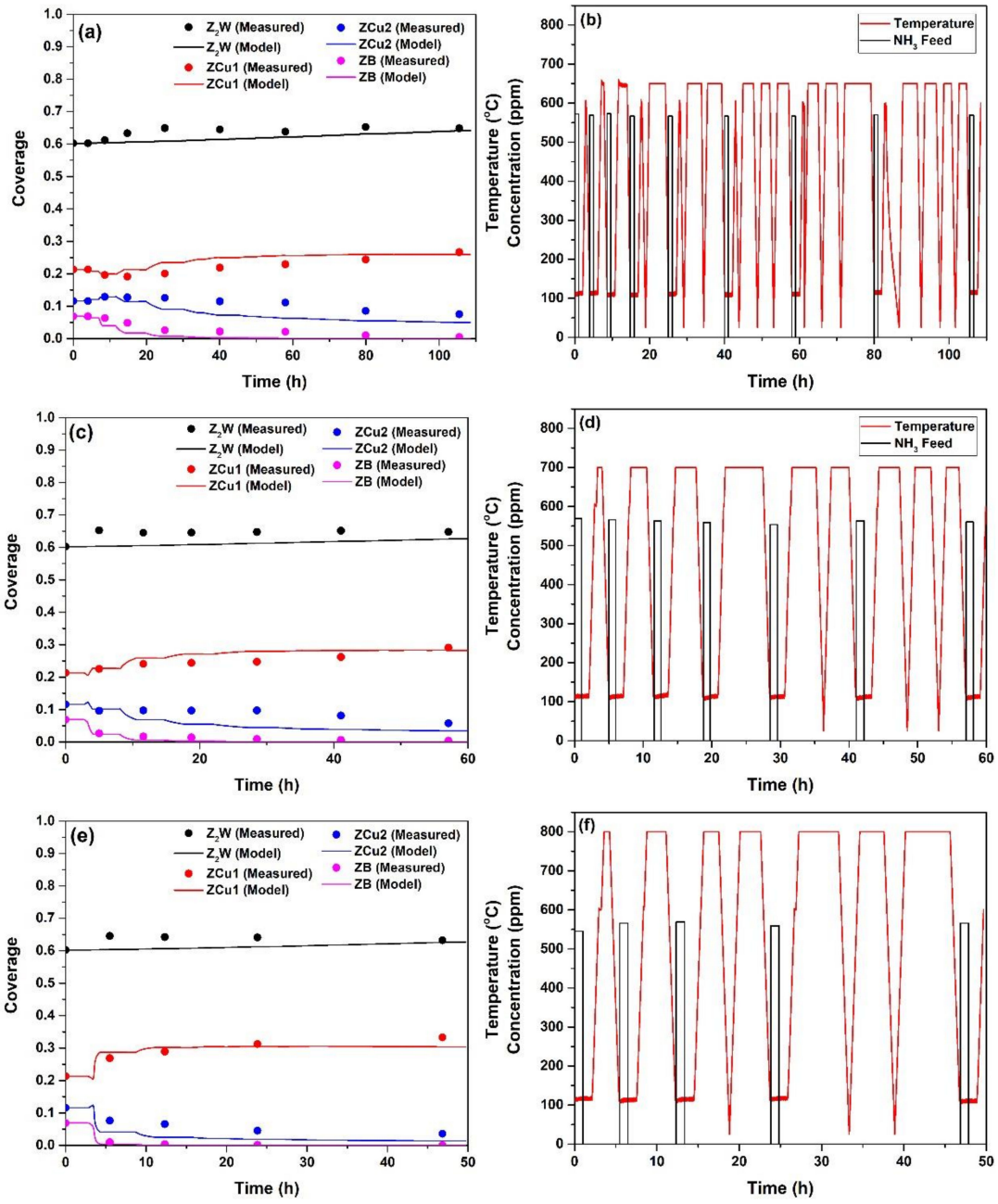

Figure 4. Measured and predicted coverage kinetics after HA at (**a**) 650 °C, (**c**) 700 °C, (**e**) 800 °C and the corresponding successive HA steps with NH_3 feed profiles of the NH_3 adsorption/TPD experiments for the HA at (**b**) 650 °C, (**d**) 700 °C, (**f**) 800 °C.

Table 1. Reactions used in the model and their rate expressions.

Reaction Number	Reaction	Rate Expression
Reactions related to HA		
1	$ZCu1 + Z \rightarrow Z_2W$	$r_1 = k_1\theta_{ZCu1}$
2	$ZCu1 + ZB \rightarrow ZCu2 + Z$	$r_2 = \frac{k_2\theta_{ZCu1}\theta_{ZB}^{n_2}}{1+K_2\theta_{ZCu2}}$
3	$ZCu2 \rightarrow ZCu1$	$r_3 = k_3\theta_{ZCu2}^{n_3}$
Reactions related to NH_3 adsorption and desorption		
4	$NH_3 + Z_2W \rightarrow Z_2WNH_3$	$r_4 = k_4C_{NH_3}\theta_{Z_2W}$
5	$Z_2WNH_3 \rightarrow NH_3 + Z_2W$	$r_5 = k_5\theta_{Z_2WNH_3}$
6	$NH_3 + ZCu1 \rightarrow ZCu1NH_3$	$r_6 = k_6C_{NH_3}\theta_{ZCu1}$
7	$ZCu1NH_3 \rightarrow NH_3 + ZCu1$	$r_7 = k_7\theta_{ZCu1NH_3}$
8	$NH_3 + ZCu2 \rightarrow ZCu2NH_3$	$r_8 = k_8C_{NH_3}\theta_{ZCu2}$
9	$ZCu2NH_3 \rightarrow NH_3 + ZCu2$	$r_9 = k_9\theta_{ZCu2NH_3}$
10	$NH_3 + ZB \rightarrow ZBNH_3$	$r_{10} = k_{10}C_{NH_3}\theta_{ZB}$
11	$ZBNH_3 \rightarrow NH_3 + ZB$	$r_{11} = k_{11}\theta_{ZBNH_3}$
Reactions related to NH_3 oxidation		
12	$4ZCu1NH_3 + 3O_2 \rightarrow 2N_2 + 6H_2O + 4ZCu1$	$r_{12} = k_{12}C_{O_2}^{n_{12}}\theta_{ZCu1NH_3}$
13	$4ZCu2NH_3 + 3O_2 \rightarrow 2N_2 + 6H_2O + 4ZCu2$	$r_{13} = k_{13}C_{O_2}^{n_{13}}\theta_{ZCu2NH_3}$

Table 2. Parameters used in the kinetic model.

Reaction Number	Turnover Rate Constant, A_j	Units of A_j	Activation Energy, $E_{A,j,0}$ ($kJ \cdot mol^{-1}$)	K_j	α/n_j
1	7.11×10^{-7}	$mol \cdot s^{-1} \cdot mol^{-1}_{site}$	7.0	-	-
2	2.00×10^{5}	$mol \cdot s^{-1} \cdot mol^{-1}_{site}$	129.7	0.48	1.7
3	3.16×10^{14}	$mol \cdot s^{-1} \cdot mol^{-1}_{site}$	280.3	-	4.3
4	1.30×10^{1}	$m^3 \cdot s^{-1} \cdot mol^{-1}_{site}$	0.0	-	-
5	8.43×10^{0}	$mol \cdot s^{-1} \cdot mol^{-1}_{site}$	16.6	-	-
6	7.04×10^{-1}	$m^3 \cdot s^{-1} \cdot mol^{-1}_{site}$	0.0	-	-
7	8.01×10^{5}	$mol \cdot s^{-1} \cdot mol^{-1}_{site}$	104.8	-	0.99
8	1.75×10^{2}	$m^3 \cdot s^{-1} \cdot mol^{-1}_{site}$	0.0	-	-
9	1.14×10^{8}	$mol \cdot s^{-1} \cdot mol^{-1}_{site}$	122.3	-	-
10	2.50×10^{2}	$m^3 \cdot s^{-1} \cdot mol^{-1}_{site}$	0.0	-	-
11	6.41×10^{7}	$mol \cdot s^{-1} \cdot mol^{-1}_{site}$	131.2	-	-
12	3.87×10^{1}	$mol^{0.75} \cdot m^{0.75} \cdot s^{-1} \cdot mol^{-1}_{site}$	61.6	-	0.25
13	2.87×10^{5}	$mol^{0.59} \cdot m^{1.77} \cdot s^{-1} \cdot mol^{-1}_{site}$	120.2	-	0.59

2.2. 4-Site Kinetic Model for Degreened Cu-CHA

In order to model the adsorption, desorption and oxidation of NH_3 over Cu-CHA from a degreened state up to a hydrothermally aged state, firstly, a transient reaction kinetics model for the degreened Cu-CHA was developed. For the adsorption and desorption of NH_3, the reactions and the associated rate expressions for each reaction are given in Table 1 (Reactions 4–11). The site densities of Z_2W, ZCu1, ZCu2 and ZB of the degreened Cu-CHA were 64.0, 45.1, 24.6 and 14.6 mol_{site}/m^3, respectively, which were obtained from NH_3 adsorption/TPD profile of the degreened catalyst. The site Z_2W occcupied two Z sites which resulted in a total Z concentration of 212.3 mol_{site}/m^3. The fractional coverages of Z_2W, ZCu1, ZCu2 and ZB for the degreened sample were, therefore, 0.60, 0.21, 0.12 and 0.07, respectively. The stoichiometry between a certain active site and NH_3 [18,47,56] was lumped into to the reaction rate parameters, similar to the prior literature [30,44]. Figure 5 shows the NH_3 concentration at the outlet of the reactor during NH_3 adsorption, isothermal desorption and TPD along with the fractional coverages obtained using the 4-site transient kinetic model for the degreened Cu-CHA. The parameters for the rate expressions of Reactions 4–11 were obtained by fitting the experimental data shown in Figure 5a to the 4-site transient kinetic model (given in Section 3.3.1) and are presented in Table 2. The model captured very well all of the vital features of the experimental data, which are the adsorption breakthrough, isothermal desorption and the TPD profiles. The peaks at 317 and 456 °C in the TPD

profile, along with the shoulder at 526 °C, were also very well predicted by the model. Here, in order for our approach to predict NH_3 storage and oxidation after HA, the kinetic model for the adsorption and desorption should be consistent with the positions of the fitted TPD peaks for the degreened catalyst (Figure 1). To elaborate, the centers of the fitted peaks (in terms of temperature) should match the temperatures where the coverages of the associated individual sites in the kinetic model are halved during TPD. Figure 5b shows the changes in the coverages of $ZCu1NH_3$, $ZCu2NH_3$, and $ZBNH_3$ species during TPD of NH_3 of the degreened Cu-CHA. During TPD, as the temperature was raised from 110 to 600 °C, NH_3 started to desorb from the aforementioned sites according to Reactions 5, 7, 9 and 11. The predicted temperatures where the coverages were halved were at 304, 451 and 513 °C for $ZCu1NH_3$, $ZCu2NH_3$ and $ZBNH_3$ (Figure 5b), respectively, which very closely match the fitted values of 317, 456 and 526 °C (Figures 1 and 2a). This shows that the kinetic model for the adsorption and desorption of NH_3 is consistent with the deconvoluted peaks of the experimental TPD curve of the degreened Cu-CHA.

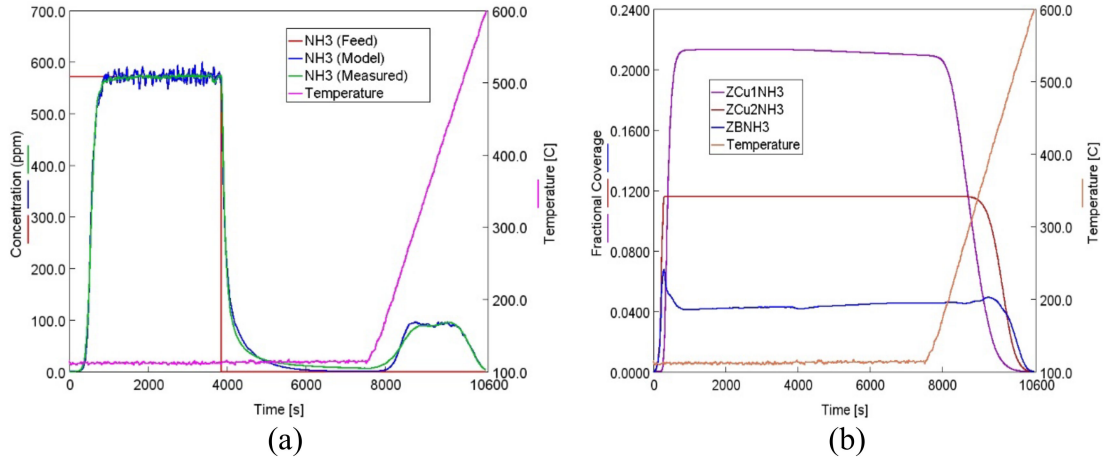

Figure 5. (**a**) Experimental and predicted NH_3 concentration during NH_3 adsorption/TPD experiment (**b**) Simulated fractional coverages of $ZCu1NH_3$, $ZCu2NH_3$, and $ZBNH_3$ at normalized axial location of 0.6 for the experiment given in (**a**).

For the development of a model for NH_3 oxidation on degreened Cu-CHA, two reactions (Reactions 12–13) were considered. The oxidation reactions were assumed to occur on ZCu1 and ZCu2 sites. The parameters for rates of NH_3 oxidation reactions were obtained by fitting transient experimental NH_3 oxidation data of the degreened Cu-CHA to the model while keeping the parameters of the rates of Reactions 4–11 constant. Parameters are presented in Table 2. The model described the NH_3 oxidation performance of the degreened catalyst very well.

2.3. Modeling the Effects of HA on NH_3 Adsorption, Desorption and Oxidation

HA resulted in various changes in the fractional coverages of the NH_3 storage sites over Cu-CHA, as previously demonstrated. These changes needed to be coupled with the 4-site transient kinetic model in order to predict the NH_3 adsorption, desorption and oxidation performance of the catalyst upon HA. Thus, the effects of HA on the adsorption and desorption was modeled using Reactions 1–11 and the effects of HA on the oxidation behavior was modeled using Reactions 1–13. The rate constants for Reactions 4–13 obtained using data for the degreened Cu-CHA were used during the simulations.

For adsorption and desorption of NH_3, Figure 6a,c,e illustrates the experimental and predicted NH_3 concentration at the outlet of the reactor, together with temperature profiles (HA treatment at 650 °C (Figure 6a), 700 °C (Figure 6c) and 800 °C (Figure 6e)). Generally, there is a very good agreement between experimental data and model predictions upon sequential HA. Figure 6b shows a comparison of experimental and predicted NH_3 concentration after 46 h of isothermal HA at 650 °C (last NH_3

adsorption/desorption experiment in Figure 6a). Model predictions agreed very well with experimental data. The increase in the intensity of the peak centered at 317 °C and the decreases in the intensity of the peaks centered at 456 and 526 °C upon HA were captured very well by the model. Figure 6d,f show a comparison of experimental and predicted NH_3 concentrations after 25 h of HA at 700 °C and 21 h of HA at 800 °C, respectively. Here, the model again described the important features of the experiment very well, including the NH_3 breakthrough, isothermal desorption and bi-modal TPD behavior of NH_3.

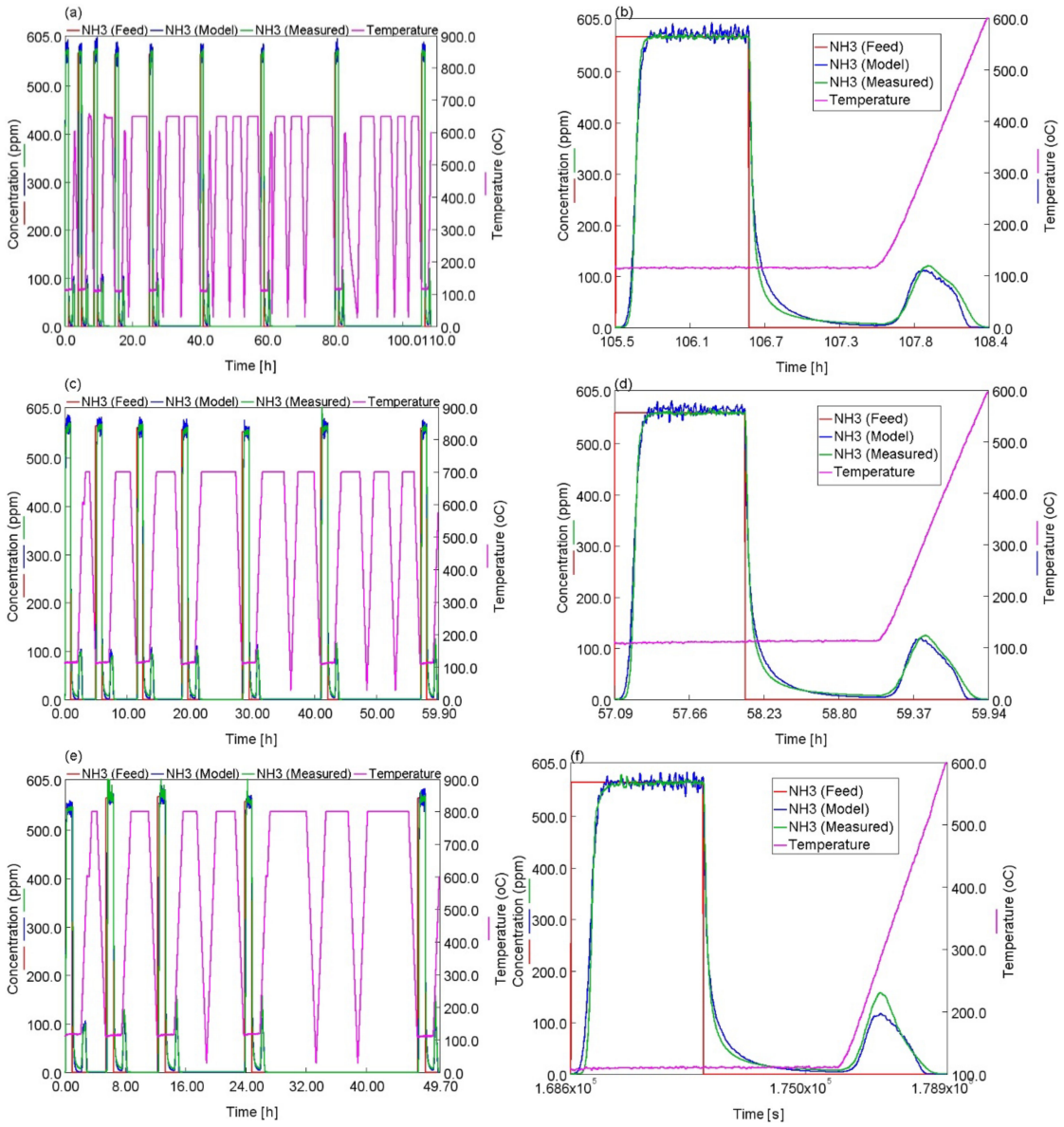

Figure 6. Temperature profiles, experimental and predicted NH_3 concentrations throughout the successive HA sets carried out at (**a**) 650 °C, (**c**) 700 °C, (**e**) 800 °C. Experimental and predicted NH_3 concentrations during the last NH_3 adsorption/TPD experiments for the HA sets carried out at (**b**) 650 °C, (**d**) 700 °C, (**f**) 800 °C.

Figure 7 shows a comparison of the measured and predicted NH_3 conversion with temperature for the degreened and aged samples for the oxidation of NH_3. Three NH_3 oxidation experiments were performed subsequent to the completion of the three HA sets carried out at 650, 700 and 800 °C, shown in Figure 6a,c,e (the conditions of aging also shown in Figure 4b,d,f). Figure 7a shows the measured and simulated data for NH_3 oxidation experiment after 46 h of isothermal HA at 650 °C.

Here, the experimental data show decreased NH_3 oxidation activity at temperatures above 330 °C, as compared to the degreened Cu-CHA. The model is in excellent agreement with the measured values. Thus, the phenomena associated with HA causing a decrease in NH_3 oxidation activity could be modeled via just accounting for the changes in the fractional coverage of NH_3 storage sites of the Cu-CHA, while keeping the turnover rate constants and the activation energies of the Reactions 12–13 obtained from the NH_3 oxidation experiment of degreened Cu-CHA unchanged. The predicted changes in the fractional coverage of storage sites upon HA are affecting the values required for Equations (3) and (12), thereby enabling the prediction of NH_3 oxidation performance after HA. Similarly, good agreement between experimental data and model predictions was obtained for NH_3 oxidation experiments after 25 h of isothermal HA at 700 °C (Figure 7b). After 21 h of isothermal HA at 800 °C (Figure 7c), the model could capture the decrease in conversion of NH_3 upon HA as compared to the degreened sample. However, the model underestimated the conversion of NH_3 at temperatures higher than 350 °C.

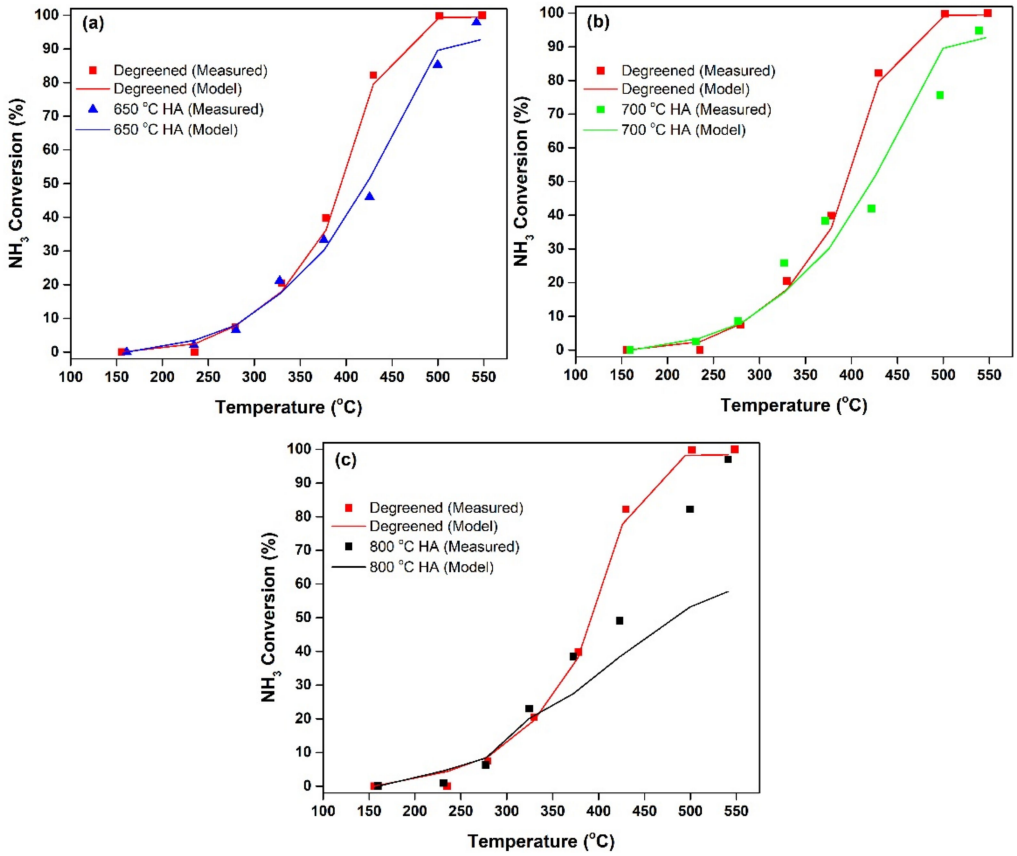

Figure 7. Variation of steady-state NH_3 conversion during NH_3 oxidation with respect to temperature for degreened and HA Cu-CHA after HA at (**a**) 650 °C, (**b**) 700 °C, (**c**) 800 °C.

The fact that the model could capture the decreases in conversion upon HA at 650 and 700 °C has several important implications. Firstly, this shows that ZCu2 was mostly responsible for the high-temperature NH_3 oxidation activity, since the decay in its coverage upon HA was well correlated with both the behavior of the TPD profile and NH_3 oxidation. Secondly, it illustrates that the HA reactions and rate expressions proposed here are valid and the aforementioned active species survive the HA treatment without forming CuO_x clusters, or if these CuO_x clusters were formed they had the same turnover rate constants. The under-estimation of the NH_3 conversion after very a high temperature HA at 800 °C could therefore be attributed to the formation of the aforementioned CuO_x clusters with different reactivites than ZCu2.

3. Materials and Methods

3.1. Laboratory Tests

The catalyst used in this study was a commercial Cu-chabazite washcoated to a cordierite monolith (300 cpsi – 5 mils). Cylindrical cores with a length of 2.2 cm and a diameter of 1.8 cm were used in the runs. The experiments were carried out in a synthetic gas bench described in [60]. In a typical run, the monolith was first wrapped with a ceramic fibre paper and then loaded in a quartz reactor and placed in the isothermal zone of an electric tubular furnace (Thermo Scientific Lindberg Blue M). The reaction temperature was monitored using a J-type thermocouple placed 0.5 cm upstream of the catalyst. NH_3, O_2, CO_2 and N_2 were delivered using calibrated mass flow controllers (Brooks Instruments) whereas H_2O was delivered using a peristaltic pump (Gilson Minipuls 3). All lines before and after the reactor were heated to 190 °C. The concentrations of the species at the outlet of the reactor were continuously monitored using a FTIR spectrometer (MKS Multigas 2030). Initially, the catalyst was degreened at 550 °C using a stream consisting of 5% H_2O and 8% O_2 in N_2 for 2h. After all of the experiments, the catalyst was hydrothermally aged, as explained below. Runs were performed with a space velocity of 40,000 h^{-1} (STP). Gases used in this study were 5.0 grade or above. NH_3 adsorption/TPD experiment included three steps, which are the adsorption, isothermal desorption, and TPD. In these experiments, NH_3 was continuously fed to the reactor for 1h at 110 °C, which resulted in an adsorption breakthrough curve. Subsequently, NH_3 feed was stopped and physisorbed NH_3 desorbed during the isothermal desorption step which continued for 1h. This was followed by a temperature ramp (10 °C/min) from 110 to 600 °C. The feed during the adsorption step was 570 ppm NH_3, 5% H_2O, 10% CO_2 in an N_2 balance. During the isothermal desorption and TPD steps, no NH_3 was fed. Fractional coverages of the NH_3 storage sites were obtained using the NH_3 adsorption, desorption and TPD experiments. TPD profiles were deconvoluted into four Gaussian peaks using Fityk software (version 1.3.1). Initially, peaks were added manually according to the experimental data. The best fits were then obtained via minimizing the weighted sum of squared residuals between the experimental data and model using Levenberg–Marquardt algorithm. For NH_3 oxidation experiments, the catalyst was exposed to a stream containing 500 ppm NH_3, 10% CO_2, 8% O_2, 5% H_2O in N_2, and temperature was increased from 155 to 540 °C in a stepwise manner. Downstream NH_3 concentration was measured. NH_3 conversion (%) at steady-state was given by $[(F_{NH3,z0}\text{-}F_{NH3,zL})/F_{NH3,z0}]x100$. The NH_3 oxidation performance of the degreened catalyst was measured for a fresh core after the degreening.

3.2. HA Methodology

HA was performed on the test rig described above. HA procedure included three sets of aging at temperatures of 650, 700 and 800 °C. All sets started with a fresh and degreened Cu-CHA sample. Thus, three fresh Cu-CHA washcoated cores were used. Once the sample was degreened, a certain HA set was started with an NH_3 adsorption/TPD experiment, as previously described in Section 3.1, to measure fractional coverages, which was followed by heating to the desired temperature (either 650, 700 or 800 °C) for an isothermal HA step for a desired time. Subsequently, the temperature was lowered to 110 °C to perform NH_3 adsorption/TPD experiment, which was again followed by heating and an isothermal HA step at the desired temperature (either 650, 700 or 800 °C) of that HA set. The above-described sequential procedure continued for up to total isothermal HA times 46, 25 and 21 h, for the isothermal HA temperatures of 650, 700 and 800 °C, respectively. The isothermal HA times accounted for the times passed at the desired isothermal HA temperature. During the sets at 650, 700 and 800 °C, 9, 7 and 5 NH_3 adsorption/TPD experiments were performed, respectively, between the HA steps, and the fractional coverages of the NH_3 storage sites were obtained accordingly after each HA step with respect to time and temperature. Heating and cooling ramps along with the isothermal HA step were carried out with a feed of 5% H_2O, 8% O_2 in N_2 balance with a space velocity of 40,000 h^{-1} (stp). NH_3 oxidation performance was measured as previously described in Section 3.1 after the completion of each set.

3.3. Modelling

3.3.1. The Reactor Model

The kinetic modelling was performed using GT-POWER, version 2018 [61]. Material balances for the modelling of NH_3 adsorption, desorption and oxidation over Cu-CHA washcoated monolith are provided below. All of the models included necessary momentum and energy balances. The length of the monolith was discretized to ten parts with uniform channels. This was sufficient to obtain data that do not vary with increasing mesh size. The unsteady-state species term for the bulk gas phase was neglected due to a very small residence time as compared to the time steps of interest.

The material balance for the species in the gas phase is

$$\varepsilon \rho_g v \frac{\partial \omega_{g,i}}{\partial z} = k_{m,i} G(\omega_{w,i} - \omega_{g,i}) \tag{1}$$

The material balance for the external mass transfer film is

$$k_{m,i} G(\omega_{w,i} - \omega_{g,i}) = R_i \tag{2}$$

$$\text{With } R_i = M_i \sum_j s_{ij} a_j r_j \tag{3}$$

$$k_{m,i} = \frac{Sh_i \rho_g D_{m,i}}{D_h} \tag{4}$$

$$G = \frac{4\varepsilon}{D_h} \tag{5}$$

The material balance for the washcoat gives

$$f_{wc} \rho_s D_{e,i} \frac{\partial^2 \omega_i}{\partial x^2} + R_i = 0 \tag{6}$$

with the flux balance at the fluid–washcoat interface in the radial direction as boundary condition

$$\rho_s D_{e,i} \left. \frac{\partial \omega_i}{\partial x} \right|_{\omega_i = \omega_{w,i}} = k_{m,i}(\omega_{w,i} - \omega_{g,i}) \text{at } x = 0 \tag{7}$$

and

$$\frac{\partial \omega_i}{\partial x} = 0 \text{ at } x = \delta \tag{8}$$

$$\text{with } \delta = \frac{f_{wc}}{S}$$

GT-POWER (version 2018) addresses the washcoat pore diffusion in a manner similar to the published literature [62]. In the model, the following expressions were utilized to obtain the effective diffusivity, Knudsen diffusivity and the binary diffusion coefficients (Fuller equation [63]).

$$\frac{1}{D_{e,i}} = \frac{\tau}{\varepsilon_w} \left(\frac{1}{D_{i,m}} + \frac{1}{D_{Kn,i}} \right) \tag{9}$$

$$D_{Kn,i} = \frac{1}{3} d_p \sqrt{\frac{8\overline{R}T}{\pi M_i}} \tag{10}$$

$$D_{i,m} = \frac{10^{-7} T^{1.75} \left(\frac{1}{M_i} + \frac{1}{M_m} \right)^{\frac{1}{2}}}{P \left((\sum V_i)^{\frac{1}{3}} + (\sum V_m)^{\frac{1}{3}} \right)^2} \tag{11}$$

The fractional coverages are given by

$$A_k \frac{d\theta_k}{dt} = \sum_j \sigma_{kj} a_j r_j \quad (12)$$

During the modelling of HA kinetics, the changes in the fractional coverages of the four storage sites were obtained using Equation (12). This is based on the assumption that there is no transport of sites in and out of the reactor, and that the sites are homogeneously dispersed, are in close-proximity to react with each other, but immobile throughout the washcoat in all directions.

3.3.2. Kinetic Model

All reactions and associated rate equations are given in Table 1. Activation energy for the adsorption reactions (Reactions 4, 6, 8 and 10) was assumed to be zero. The temperature dependence of the turnover rate constant, k_j was given by the Arrhenius equation

$$k_j = A_j e^{\frac{-E_{A,j}}{RT}} \quad (13)$$

where A_j is the turnover rate constant and $E_{A,j}$ is the activation energy in reaction j. A coverage-dependent activation energy function was used to describe the desorption of NH_3 in Reaction 7:

$$E_{A,j} = E_{A,j,0}(1 - \alpha\theta_{S-NH_3}) \quad (14)$$

HA kinetics model parameters were optimized in GT-POWER to minimize the sum of squared error between the experimental data for fractional coverages obtained via deconvolution of the TPD profiles and the fractional coverages calculated by the model via a genetic algorithm. Equation (12) and rate expressions of the Reactions 1–3 given in Table 1 were used. The effects of gaseous species (O_2 and H_2O) concentrations during HA were neglected since the HA experiments were carried out with a feed which includes O_2 and H_2O to represent the general cases of HA in an engine ATS, and also not to further complicate the model. For this purpose, the HA aging sets given in Figure 4b,d,f, with durations of 109, 60 and 50 h (i.e., totals of 46, 25 and 21 h isothermal HA, heating and cooling ramps and for NH_3 adsorption and TPD experiments) for 650, 700 and 800 °C aging sets, respectively, were utilized. Thus, not only the isothermal parts of HA but also the associated heating and cooling ramps were considered during the development of the HA kinetics model and its kinetic parameter optimization process.

The parameters of rate expressions of Reactions 4–11 were also optimized in GT-POWER using the experimental NH_3 adsorption/TPD data of the degreened catalyst via a genetic algorithm. Parameters of the rate expressions of Reactions 12 and 13 were obtained using the experimental data of NH_3 oxidation for the degreened catalyst while keeping the parameters of Reactions 4–11 constant. Then, the HA kinetics model and the model for the adsorption and desorption of NH_3 was linked through the utilization of Equations (1)–(14), and along with Reactions 1–11, to describe the NH_3 adsorption and desorption after a certain HA treatment. The HA kinetics model was linked to the models of NH_3 adsorption, desorption and oxidation through the utilization of Equations (1)–(14) and Reactions 1–13.

4. Conclusions

An accurate HA kinetics model of the changes in the fractional coverages of the four NH_3 storage sites of the Cu-CHA with respect to HA time and temperature was developed based on NH_3-TPD profile deconvolutions. The main conclusions are as the following:

- HA kinetics model successfully captured the changes in the fractional coverages of the NH_3 storage sites, which could be identified with their NH_3-TPD peak centres observed at 317, 456 and 526 °C, namely ZCu1, ZCu2 and ZB, respectively, for the degreened catalyst. The fractional

coverages of ZCu2 and ZCu1 initially increased and decreased, respectively, with HA time after isothermal HA at 650 °C, which was well represented by the HA kinetics model. The major effects of HA were the decrease in the fractional coverages of ZCu2 and ZB and the increase in the fractional coverage of ZCu1 with further increases in both HA time and temperature. These effects were also well captured by the model;

- HA kinetics model was then linked with a 4-site transient kinetic model of adsorption, desorption and oxidation of NH_3 developed for degreened Cu-CHA. This linkage was possible via incorporating the changes in the fractional coverages of the NH_3 storage sites to the coverages of the active sites within the reactor model through the utilization of HA kinetics, while keeping the turnover rate constants and the activation energies associated with reactions occurring on the degreened catalysts unchanged;
- The kinetic model is able to describe the kinetics of NH_3 adsorption and isothermal desorption of NH_3, TPD of NH_3 and NH_3 oxidation of the degreened and hydrothermally aged Cu-CHA up to 46, 24 and 21 h at 650, 700 and 800 °C, respectively. The decreases in high temperature NH_3 oxidation performance upon HA, at 650 °C for 46 h and at 700 °C for 24 h were very well predicted by the model;
- Both the HA methodology and the method used to create a link between the HA kinetics and the reaction models developed in this study could be extended to a variety of other catalytic systems for the prediction catalytic activity after HA. Along this line, the development of an HA model capable of describing the NH_3-SCR performance after mild HA is on-going in our laboratory.

Author Contributions: S.E.B. and C.E. designed the study and wrote the paper. S.E.B. carried out the experiments, analysed the data and developed the aging model. S.E.B., D.Ş., B.Ö., G.H. and C.E. edited and reviewed the paper. G.H. and C.E. supervised the whole project. All authors have read and agreed to the published version of the manuscript.

Funding: This research received funding from Ford Otomotiv Sanayi A.Ş.

Conflicts of Interest: The authors declare no conflict of interest.

Nomenclature

a_j	Active site concentration for reaction j, ($mol_{site}·m^{-3}$·catalyst)
A_k	Active site concentration for coverage k, ($mol·m^{-3}$·catalyst)
A_j	Turnover rate constant for reaction j
C_i	Intraporous concentration of species i ($mol·m^{-3}$)
$D_{i,m}$	Binary diffusion coefficient of species i in the mixture ($m^2·s^{-1}$)
$D_{e,i}$	Effective diffusivity for species i ($m^2·s^{-1}$)
$D_{Kn,i}$	Knudsen diffusion coefficient for species i ($m^2·s^{-1}$)
D_h	Hydraulic diameter (m)
d_p	Washcoat pore size available for gas diffusion (m)
$E_{A,j}$	Activation energy for reaction j ($kJ·mol^{-1}$)
$E_{A,j,0}$	Activation energy for reaction j at zero coverage ($kJ·mol^{-1}$)
$F_{i,z0}$	Molar flow rate of species i at $z = 0$
$F_{i,zL}$	Molar flow rate of species i at $z = L$
f_{wc}	Solid fraction of washcoat
G	Surface area per reactor volume (m^{-1})
k_j	Turnover rate constant for the reaction j
$k_{m,i}$	External mass transfer coefficient for species i ($kg·m^{-2}$ s^{-1})
L	Reactor length
M_i	Molecular weight of species i ($kg·mol^{-1}$)
r_j	Reaction rate for reaction j ($mol·s^{-1}·mol_{site}{}^{-1}$)
R	Gas constant ($J·mol^{-1}·K^{-1}$)
R_i	Species mass rate for generation or consumption ($kg·m^{-3}·s^{-1}$)

s_{ij}	Stoichiometric coefficient of species i for reaction j
Sh_i	Sherwood number
V_i	Diffusion volume for species i ($cm^3 \cdot mol^{-1}$)
v	Interstitial velocity ($m \cdot s^{-1}$)
Greek letters	
α	Coverage dependence
δ	Washcoat thickness (m)
ε	Void fraction of reactor
ε_w	Void fraction of washcoat
ρ_g	Density of bulk gas in reactor channels ($kg \cdot m^{-3}$)
ρ_s	Density of gas at catalyst surface ($kg \cdot m^{-3}$)
ω_i	Intraporous mass fraction of species i
$\omega_{g,i}$	Mass fraction of species i in the bulk gas
$\omega_{w,i}$	Mass fraction of species i in the gas-solid interface
θ_k	Fractional coverage of species k
σ_{kj}	Stoichiometric coefficient of species j in reaction k

References

1. Kwak, J.H.; Tonkyn, R.G.; Kim, D.H.; Szanyi, J.; Peden, C.H.F. Excellent activity and selectivity of Cu-SSZ-13 in the selective catalytic reduction of NOx with NH_3. *J. Catal.* **2010**, *275*, 187–190. [CrossRef]
2. Depcik, C.; Assanis, D. One-dimensional automotive catalyst modeling. *Progr. Energy Combust. Sci.* **2005**, *31*, 308–369. [CrossRef]
3. Chatterjee, D.; Burkhardt, T.; Bandl-Konrad, B.; Braun, T.; Tronconi, E.; Nova, I.; Ciardelli, C. Numerical Simulation of Ammonia SCR-Catalytic Converters: Model Development and Application. *SAE Tech. Paper Ser.* **2005**, *114*, 437–448.
4. Chatterjee, D.; Burkhardt, T.; Weibel, M.; Nova, I.; Grossale, A.; Tronconi, E. Numerical Simulation of Zeolite- and V-Based SCR Catalytic Converters 2007-01-1136. *SAE Tech. Paper Ser.* **2007**. [CrossRef]
5. Schmieg, S.J.; Oh, S.H.; Kim, C.H.; Brown, D.B.; Lee, J.H.; Peden, C.H.F.; Kim, D.H. Thermal durability of Cu-CHA NH3-SCR catalysts for diesel NOx reduction. *Catal. Today* **2012**, *184*, 252–261. [CrossRef]
6. Ma, L.; Cheng, Y.; Cavataio, G.; McCabe, R.W.; Fu, L.; Li, J. Characterization of commercial Cu-SSZ-13 and Cu-SAPO-34 catalysts with hydrothermal treatment for NH3-SCR of NOx in diesel exhaust. *Chem. Eng. J.* **2013**, *225*, 323–330. [CrossRef]
7. Luo, J.; Wang, D.; Kumar, A.; Li, J.; Kamasamudram, K.; Currier, N.; Yezerets, A. Identification of two types of Cu sites in Cu/SSZ-13 and their unique responses to hydrothermal aging and sulfur poisoning. *Catal. Today* **2016**, *267*, 3–9. [CrossRef]
8. Luo, J.; An, H.; Kamasamudram, K.; Currier, N.W.; Yezerets, A.; Watkins, T.; Allard, L. Impact of Accelerated Hydrothermal Aging on Structure and Performance of Cu-SSZ-13 SCR Catalysts. *SAE Int. J. Engines* **2015**, *8*, 1181–1186. [CrossRef]
9. Han, S.; Ye, Q.; Cheng, S.; Kang, T.; Dai, H. Effect of the hydrothermal aging temperature and Cu/Al ratio on the hydrothermal stability of CuSSZ-13 catalysts for NH3-SCR. *Catal. Sci. Technol.* **2017**, *7*, 703–717. [CrossRef]
10. Gao, F.; Walter, E.D.; Karp, E.M.; Luo, J.Y.; Tonkyn, R.G.; Kwak, J.H.; Szanyi, J.; Peden, C.H.F. Structure-activity relationships in NH3-SCR over Cu-SSZ-13 as probed by reaction kinetics and EPR studies. *J. Catal.* **2013**, *300*, 20–29. [CrossRef]
11. Kwak, J.H.; Tran, D.; Szanyi, J.; Peden, C.H.F.; Lee, J.H. The Effect of Copper Loading on the Selective Catalytic Reduction of Nitric Oxide by Ammonia Over Cu-SSZ-13. *Catal. Lett.* **2012**, *142*, 295–301. [CrossRef]
12. Gao, F.; Washton, N.M.; Wang, Y.; Kollár, M.; Szanyi, J.; Peden, C.H.F. Effects of Si/Al ratio on Cu/SSZ-13 NH3-SCR catalysts: Implications for the active Cu species and the roles of Brønsted acidity. *J. Catal.* **2015**, *331*, 25–38. [CrossRef]
13. Gao, F.; Walter, E.D.; Kollar, M.; Wang, Y.L.; Szanyi, J.; Peden, C.H.F. Understanding ammonia selective catalytic reduction kinetics over Cu/SSZ-13 from motion of the Cu ions. *J. Catal.* **2014**, *319*, 1–14. [CrossRef]
14. Wang, L.; Li, W.; Qi, G.S.; Weng, D. Location and nature of Cu species in Cu/SAPO-34 for selective catalytic reduction of NO with NH3. *J. Catal.* **2012**, *289*, 21–29. [CrossRef]

15. Wang, D.; Zhang, L.; Li, J.H.; Kamasamudram, K.; Epling, W.S. NH3-SCR over Cu/SAPO-34—Zeolite acidity and Cu structure changes as a function of Cu loading. *Catal. Today* **2014**, *231*, 64–74. [CrossRef]
16. Bates, S.A.; Verma, A.A.; Paolucci, C.; Parekh, A.A.; Anggara, T.; Yezerets, A.; Schneider, W.F.; Miller, J.T.; Delgass, W.N.; Ribeiro, F.H. Identification of the active Cu site in standard selective catalytic reduction with ammonia on Cu-SSZ-13. *J. Catal.* **2014**, *312*, 87–97. [CrossRef]
17. Groothaert, M.H.; Van Bokhoven, J.A.; Battiston, A.A.; Weckhuysen, B.M.; Schoonheydt, R.A. Bis(mu-oxo)dicopper in Cu-ZSM-5 and its role in the decomposition of NO: A combined in situ XAFS, UV-Vis-Near-IR, and kinetic study. *J. Am. Chem. Soc.* **2003**, *125*, 7629–7640. [CrossRef] [PubMed]
18. Paolucci, C.; Khurana, I.; Parekh, A.A.; Li, S.; Shih, A.J.; Li, H.; Di Iorio, J.R.; Albarracin-Caballero, J.D.; Yezerets, A.; Miller, J.T.; et al. Dynamic multinuclear sites formed by mobilized copper ions in NOx selective catalytic reduction. *Science* **2017**, *357*, 898–903. [CrossRef] [PubMed]
19. Wang, D.; Zhang, L.; Kamasamudram, K.; Epling, W.S. In Situ-DRIFTS Study of Selective Catalytic Reduction of NOx by NH3 over Cu-Exchanged SAPO-34. *ACS Catal.* **2013**, *3*, 871–881. [CrossRef]
20. Giordanino, F.; Vennestrom, P.N.R.; Lundegaard, L.F.; Stappen, F.N.; Mossin, S.; Beato, P.; Bordiga, S.; Lamberti, C. Characterization of Cu-exchanged SSZ-13: A comparative FTIR, UV-Vis, and EPR study with Cu-ZSM-5 and Cu-beta with similar Si/Al and Cu/Al ratios. *Dalton Trans.* **2013**, *42*, 12741–12761. [CrossRef]
21. Borfecchia, E.; Lomachenko, K.A.; Giordanino, F.; Falsig, H.; Beato, P.; Soldatov, A.V.; Bordiga, S.; Lamberti, C. Revisiting the nature of Cu sites in the activated Cu-SSZ-13 catalyst for SCR reaction. *Chem. Sci.* **2015**, *6*, 548–563. [CrossRef] [PubMed]
22. Janssens, T.V.W.; Falsig, H.; Lundegaard, L.F.; Vennestrom, P.N.R.; Rasmussen, S.B.; Moses, P.G.; Giordanino, F.; Borfecchia, E.; Lomachenko, K.A.; Lamberti, C.; et al. A Consistent Reaction Scheme for the Selective Catalytic Reduction of Nitrogen Oxides with Ammonia. *ACS Catal.* **2015**, *5*, 2832–2845. [CrossRef]
23. Paolucci, C.; Parekh, A.A.; Khurana, I.; Di Iorio, J.R.; Li, H.; Albarracin Caballero, J.D.; Shih, A.J.; Anggara, T.; Delgass, W.N.; Miller, J.T.; et al. Catalysis in a Cage: Condition-Dependent Speciation and Dynamics of Exchanged Cu Cations in SSZ-13 Zeolites. *J. Am. Chem. Soc.* **2016**, *138*, 6028–6048. [CrossRef] [PubMed]
24. Ipek, B.; Wulfers, M.J.; Kim, H.; Göltl, F.; Hermans, I.; Smith, J.P.; Booksh, K.S.; Brown, C.M.; Lobo, R.F. Formation of $[Cu_2O_2]^{2+}$ and $[Cu_2O]^{2+}$ toward C–H Bond Activation in Cu-SSZ-13 and Cu-SSZ-39. *ACS Catal.* **2017**, *7*, 4291–4303. [CrossRef]
25. Rizzotto, V.; Chen, P.; Simon, U. Mobility of NH3-Solvated CuII Ions in Cu-SSZ-13 and Cu-ZSM-5 NH3-SCR Catalysts: A Comparative Impedance Spectroscopy Study. *Catalysts* **2018**, *8*, 162. [CrossRef]
26. Marberger, A.; Petrov, A.W.; Steiger, P.; Elsener, M.; Kröcher, O.; Nachtegaal, M.; Ferri, D. Time-resolved copper speciation during selective catalytic reduction of NO on Cu-SSZ-13. *Nat. Catal.* **2018**, *1*, 221–227. [CrossRef]
27. Fahami, A.R.; Günter, T.; Doronkin, D.E.; Casapu, M.; Zengel, D.; Vuong, T.H.; Simon, M.; Breher, F.; Kucherov, A.V.; Brückner, A.; et al. The dynamic nature of Cu sites in Cu-SSZ-13 and the origin of the seagull NOx conversion profile during NH3-SCR. *React. Chem. Eng.* **2019**, *4*, 1000–1018. [CrossRef]
28. Leistner, K.; Kumar, A.; Kamasamudram, K.; Olsson, L. Mechanistic study of hydrothermally aged Cu/SSZ-13 catalysts for ammonia-SCR. *Catal. Today* **2018**, *307*, 55–64. [CrossRef]
29. Leistner, K.; Xie, K.; Kumar, A.; Kamasamudram, K.; Olsson, L. Ammonia Desorption Peaks Can Be Assigned to Different Copper Sites in Cu/SSZ-13. *Catal. Lett.* **2017**, *147*, 1882–1890. [CrossRef]
30. Olsson, L.; Wijayanti, K.; Leistner, K.; Kumar, A.; Joshi, S.Y.; Kamasamudram, K.; Currier, N.W.; Yezerets, A. A multi-site kinetic model for NH3-SCR over Cu/SSZ-13. *Appl. Catal. B Environ.* **2015**, *174*, 212–224. [CrossRef]
31. Olsson, L.; Sjovall, H.; Blint, R.J. A kinetic model for ammonia selective catalytic reduction over Cu-ZSM-5. *Appl. Catal. B Environ.* **2008**, *81*, 203–217. [CrossRef]
32. Metkar, P.S.; Balakotaiah, V.; Harold, M.P. Experimental and kinetic modeling study of NO oxidation: Comparison of Fe and Cu-zeolite catalysts. *Catal. Today* **2012**, *184*, 115–128. [CrossRef]
33. Metkar, P.S.; Harold, M.P.; Balakotaiah, V. Selective catalytic reduction of NOx on combined Fe- and Cu-zeolite monolithic catalysts: Sequential and dual layer configurations. *Appl. Catal. B Environ.* **2012**, *111*, 67–80. [CrossRef]
34. Joshi, S.Y.; Kumar, A.; Luo, J.; Kamasamudram, K.; Currier, N.W.; Yezerets, A. Combined experimental and kinetic modeling study of the bi-modal NOx conversion profile on commercial Cu-SAPO-34 catalyst under standard SCR conditions. *Appl. Catal. B Environ.* **2015**, *165*, 27–35. [CrossRef]

35. Roduit, B.; Wokaun, A.; Baiker, A. Global Kinetic Modeling of Reactions occurring during Selective Catalytic Reduction of NO by NH3 over Vanadia/Titania-Based Catalysts. *Ind. Eng. Chem. Res.* **1998**, *37*, 4577–4590. [CrossRef]
36. Bozbağ, S.E.; Şimşek, M.; Demir, O.; Şanlı, D.; Ozener, B.; Hisar, G.; Erkey, C. Assessment of the Single-Site Kinetic Model for NH3-SCR on Cu-Chabazite for the Prediction of NOx Emissions in Dynamometer Tests. *Emiss. Control Sci. Technol.* **2019**. [CrossRef]
37. Colombo, M.; Nova, I.; Tronconi, E. Detailed kinetic modeling of the NH3-NO/NO2 SCR reactions over a commercial Cu-zeolite catalyst for Diesel exhausts after treatment. *Catal. Today* **2012**, *197*, 243–255. [CrossRef]
38. Bendrich, M.; Scheuer, A.; Hayes, R.E.; Votsmeier, M. Unified mechanistic model for Standard SCR, Fast SCR, and NO_2 SCR over a copper chabazite catalyst. *Appl. Catal. B Environ.* **2018**, *222*, 76–87. [CrossRef]
39. Zhong, C.; Gong, J.; Tan, L.; Liu, W.; Liu, G.; Zhang, Z. Modeling intraphase and interphase mass transfer limitations for NH_3–SCR over Cu–ZSM–5. *Chem. Eng. Sci.* **2019**, *207*, 479–489. [CrossRef]
40. Auvray, X.; Partridge, W.; Choi, J.-S.; Pihl, J.; Coehlo, F.; Yezerets, A.; Kamasamudram, K.; Currier, N.; Olsson, L. Kinetic modeling of NH3-SCR over a supported Cu zeolite catalyst using axial species distribution measurements. *Appl. Catal. B Environ.* **2015**, *163*, 393–403. [CrossRef]
41. Dhillon, P.S.; Harold, M.P.; Wang, D.; Kumar, A.; Joshi, S.Y. Modeling and analysis of transport and reaction in washcoated monoliths: Cu-SSZ-13 SCR and dual-layer Cu-SSZ-13 + Pt/Al_2O_3 ASC. *React. Chem. Eng.* **2019**, *4*, 1103–1115. [CrossRef]
42. Joshi, S.Y.; Kumar, A.; Luo, J.; Kamasamudram, K.; Currier, N.W.; Yezerets, A. New insights into the mechanism of NH3-SCR over Cu- and Fe-zeolite catalyst: Apparent negative activation energy at high temperature and catalyst unit design consequences. *App. Catal. B Environ.* **2018**, *226*, 565–574. [CrossRef]
43. De-La-Torre, U.; Pereda-Ayo, B.; Gutiérrez-Ortiz, M.A.; González-Marcos, J.A.; González-Velasco, J.R. Steady-state NH_3-SCR global model and kinetic parameter estimation for NOx removal in diesel engine exhaust aftertreatment with Cu/chabazite. *Catal. Today* **2017**, *296*, 95–104. [CrossRef]
44. Daya, R.; Desai, C.; Vernham, B. Development and Validation of a Two-Site Kinetic Model for NH3-SCR over Cu-SSZ-13. Part 1. Detailed Global Kinetics Development Based on Mechanistic Considerations. *Emiss. Control Sci. Technol.* **2018**, *4*, 143–171. [CrossRef]
45. Sjovall, H.; Blint, R.J.; Olsson, L. Detailed kinetic modeling of NH3 SCR over Cu-ZSM-5. *Appl. Catal. B Environ.* **2009**, *92*, 138–153. [CrossRef]
46. Jangjou, Y.; Sampara, C.S.; Gu, Y.; Wang, D.; Kumar, A.; Li, J.; Epling, W.S. Mechanism-based kinetic modeling of Cu-SSZ-13 sulfation and desulfation for NH3-SCR applications. *React. Chem. Eng.* **2019**, *4*, 1038–1049. [CrossRef]
47. Villamaina, R.; Liu, S.; Nova, I.; Tronconi, E.; Ruggeri, M.P.; Collier, J.; York, A.; Thompsett, D. Speciation of Cu Cations in Cu-CHA Catalysts for NH_3-SCR: Effects of SiO_2/AlO_3 Ratio and Cu-Loading Investigated by Transient Response Methods. *ACS Catal.* **2019**, *9*, 8916–8927. [CrossRef]
48. Supriyanto; Wijayanti, K.; Kumar, A.; Joshi, S.; Kamasamudram, K.; Currier, N.W.; Yezerets, A.; Olsson, L. Global kinetic modeling of hydrothermal aging of NH_3-SCR over Cu-zeolites. *Appl. Catal. B Environ.* **2015**, *163*, 382–392. [CrossRef]
49. Ruggeri, M.P.; Nova, I.; Tronconi, E.; Schmeißer, V.; Weibel, M. Modelling the Hydrothermal Ageing of a Fe-Zeolite Catalyst for Automotive NH3-SCR Applications. *Chem. Ing. Tech.* **2018**, *90*, 803–815. [CrossRef]
50. Song, J.; Wang, Y.; Walter, E.D.; Washton, N.M.; Mei, D.; Kovarik, L.; Engelhard, M.H.; Prodinger, S.; Wang, Y.; Peden, C.H.F.; et al. Toward Rational Design of Cu/SSZ-13 Selective Catalytic Reduction Catalysts: Implications from Atomic-Level Understanding of Hydrothermal Stability. *ACS Catal.* **2017**, *7*, 8214–8227. [CrossRef]
51. Albarracin-Caballero, J.D.; Khurana, I.; Di Iorio, J.R.; Shih, A.J.; Schmidt, J.E.; Dusselier, M.; Davis, M.E.; Yezerets, A.; Miller, J.T.; Ribeiro, F.H.; et al. Structural and kinetic changes to small-pore Cu-zeolites after hydrothermal aging treatments and selective catalytic reduction of NOx with ammonia. *React. Chem. Eng.* **2017**, *2*, 168–179. [CrossRef]
52. Fan, C.; Chen, Z.; Pang, L.; Ming, S.; Zhang, X.; Albert, K.B.; Liu, P.; Chen, H.; Li, T. The influence of Si/Al ratio on the catalytic property and hydrothermal stability of Cu-SSZ-13 catalysts for NH_3-SCR. *Appl. Catal. A Gen.* **2018**, *550*, 256–265. [CrossRef]

53. Schmidt, J.E.; Oord, R.; Guo, W.; Poplawsky, J.D.; Weckhuysen, B.M. Nanoscale tomography reveals the deactivation of automotive copper-exchanged zeolite catalysts. *Nat. Commun.* **2017**, *8*, 1666. [CrossRef] [PubMed]
54. Wang, J.; Peng, Z.; Qiao, H.; Han, L.; Bao, W.; Chang, L.; Feng, G.; Liu, W. Influence of aging on in situ hydrothermally synthesized Cu-SSZ-13 catalyst for NH3-SCR reaction. *RSC Adv.* **2014**, *4*, 42403–42411. [CrossRef]
55. Kim, Y.J.; Lee, J.K.; Min, K.M.; Hong, S.B.; Nam, I.-S.; Cho, B.K. Hydrothermal stability of CuSSZ13 for reducing NOx by NH_3. *J. Catal.* **2014**, *311*, 447–457. [CrossRef]
56. Luo, J.; Gao, F.; Kamasamudram, K.; Currier, N.; Peden, C.H.F.; Yezerets, A. New insights into Cu/SSZ-13 SCR catalyst acidity. Part I: Nature of acidic sites probed by NH3 titration. *J. Catal.* **2017**, *348*, 291–299. [CrossRef]
57. Luo, J.; Kamasamudram, K.; Currier, N.; Yezerets, A. NH3-TPD methodology for quantifying hydrothermal aging of Cu/SSZ-13 SCR catalysts. *Chem. Eng. Sci.* **2018**, *190*, 60–67. [CrossRef]
58. Daya, R.; Joshi, S.Y.; Luo, J.; Dadi, R.K.; Currier, N.W.; Yezerets, A. On kinetic modeling of change in active sites upon hydrothermal aging of Cu-SSZ-13. *Appl. Catal. B Environ.* **2020**, *263*, 118368. [CrossRef]
59. Karadag, G.H. Three-site Kinetic Model for Selective Catalytic Reduction of NO_X with Ammonia over a Commercial Catalyst for Calibration of Aftertreatment Systems in Diesel Powered Heavy Duty Vehicles. Ph.D. Thesis, Koç University, Istanbul, Turkey, 2017.
60. Karadag, H.G.; Bozbag, S.E.; Şanli, D.; Demir, O.; Ozener, B.; Hisar, G.; Erkey, C. Mass Transfer Effects in SCR Reactor for NOx Abatement in Diesel Engines. In *Exergetic, Energetic and Environmental Dimensions*; Dincer, I., Colpan, C.O., Kizilkan, O., Eds.; Academic Press: Cambridge, MA, USA, 2018; pp. 961–979. [CrossRef]
61. *GT-SUITE Exhaust Aftertreatment Application Manual*; Gamma Technologies LLC.: Westmont, IL, USA, 2018.
62. Bissett, E.J. An Asymptotic Solution for Washcoat Pore Diffusion in Catalytic Monoliths. *Emiss. Control Sci. Technol.* **2015**, *1*, 3–16. [CrossRef]
63. Fuller, E.N.; Schettler, P.D.; Giddings, J.C. A New Method for Prediciton of Binary Gas-Phase Diffusion Coefficients. *Ind. Eng. Chem.* **1966**, *58*, 19–27.